Surface & Coatings Technology 532 (2026) 133610

Contents lists available at ScienceDirect

Surface & Coatings Technology

journal homepage: www.elsevier.com/locate/surfcoat

Lysine-functionalized polyglutamate copolymer nanofibers with intrinsic cell-adhesiveness and drug delivery capability for neural regeneration☆

Yu-Ting Lin [a,b], Wei-Fang Su [a], Yu-Sheng Hsiao [b,*], Chun-Yu Chang [c], Meng-Fang Lin [a,*], Yu-Ching Huang [a,d,**]

[a] Department of Materials Engineering & Biochemical Technology R&D Center, Ming Chi University of Technology, New Taipei City, 24301, Taiwan
[b] Department of Materials Science and Engineering, National Taiwan University of Science and Technology, Taipei, 10607, Taiwan
[c] Bachelor Program in Semiconductor Materials and Fabrication, Ming Chi University of Technology, New Taipei City, 24301, Taiwan
[d] Department of Chemical and Materials Engineering, Chang Gung University, Taoyuan, 33302, Taiwan

ARTICLE INFO

Keywords:
Neuron
Tissue engineering
Polypeptide
Cpolymer
Scaffold
Drug release
Neurite outgrowth
Central nervous system, regeneration

ABSTRACT

The clinical management of central nervous system (CNS) injuries remains limited by the poor regenerative capacity of neurons and the transient efficacy of neuroprotective agents. Herein, we report a novel electrospun nanofiber scaffold based on a lysine-functionalized poly(γ-benzyl-L-glutamate) *co*polymer, P((CBZL)$_m$-co-(BG)$_n$), that integrates structural biomimicry and drug delivery in a single platform. Through precise composition control (CBZL:BG = 7:3), the scaffold exhibits improved hydrophilicity, mechanical integrity, and intrinsic cell-adhesive properties, eliminating the need for additional coatings. Minocycline hydrochloride (MH), a potent neuroprotective agent, was successfully loaded up to 6 wt%. In vitro release studies revealed a three-phase sustained release profile spanning 14 days, which maintained drug activity while minimizing burst-induced cytotoxicity. Neural cell assays confirmed enhanced cell adhesion, viability, and neurite outgrowth, with maximum neurite length up to 214 μm after 7 day culture. These results underscore the potential of our copolymeric scaffolds as an effective CNS regenerative platform, offering concurrent support for cell guidance and controlled therapeutic delivery.

1. Introduction

The nervous system is divided into the central nervous system (CNS) and the peripheral nervous system (PNS) [1]. The CNS, comprising the brain and spinal cord, governs most bodily functions, whereas the PNS transmits sensory and motor signals between the CNS and peripheral tissues [2]. Due to the complex architecture and poor regenerative capacity of the CNS, injuries such as stroke, traumatic brain injury, spinal cord injury, and neurodegenerative disorders like Alzheimer's and Parkinson's disease often result in permanent neurological deficits [3]. These conditions pose significant therapeutic challenges, as CNS neurons exhibit extremely limited self-repair capability. Neural tissue engineering has emerged as a promising strategy to overcome these limitations [4,5], aiming to create biomimetic scaffolds that support neuronal growth, differentiation [6], and regeneration. Ideal scaffolds should exhibit biocompatibility to prevent immune rejection, as well as mechanical robustness and suitable elasticity to accommodate the dynamic environment of neural tissues [7]. Furthermore, scaffolds must promote neuronal adhesion and neurite outgrowth by providing a favorable extracellular microenvironment.

Restoring functional recovery following CNS injury remains a critical challenge in regenerative medicine, owing to the limited regenerative capacity of neurons and the complexity of the post-injury microenvironment [8]. Among therapeutic strategies, the use of neuroprotective drugs has shown promise in enhancing neuronal survival, reducing inflammation, and supporting axonal regrowth [9–11]. Minocycline hydrochloride (MH), a second-generation tetracycline derivative, is widely studied for its anti-inflammatory and neuroprotective properties and has been shown to potentiate the effects of nerve growth factor (NGF) on neurite outgrowth in PC12 cells [12,13]. However, its clinical application is hindered by a relatively short systemic half-life (~16 h) following oral or intravenous administration [14], necessitating the

☆ This article is part of a Special issue entitled: 'TACT2025' published in Surface & Coatings Technology.

* Corresponding authors.
** Correspondence to: Y.-C. Huang, Department of Chemical and Materials Engineering, Chang Gung University, Taoyuan, 33302, Taiwan.
E-mail addresses: yshsiao@mail.ntust.edu.tw (Y.-S. Hsiao), mflin@mail.mcut.edu.tw (M.-F. Lin), huangyc@mail.mcut.edu.tw (Y.-C. Huang).

https://doi.org/10.1016/j.surfcoat.2026.133610
Received 10 December 2025; Received in revised form 26 April 2026; Accepted 18 May 2026
Available online 25 May 2026

development of a controlled and sustained release system to maintain therapeutic concentrations at the injury site [15–17]. Electrospun nanofiber scaffolds have emerged as promising drug carriers due to their high surface area, tunable porosity, and ability to mimic the architecture of native extracellular matrix (ECM) [18,19]. These scaffolds enable localized and sustained drug delivery [20,21], which is particularly advantageous for long-term CNS treatment by reducing systemic toxicity and maintaining bioactivity [22,23]. Previous studies demonstrated that poly(γ-benzyl-L-glutamate) (PBG) [24] can successfully encapsulate ~4 wt% of MH and promote neurite extension [25–27]. However, the hydrophobic nature of PBG results in poor hydrophilicity, limited cell adhesion, and suboptimal drug dispersion. As Wu and Liu et al. have shown, scaffold hydrophilicity strongly influences initial burst release behavior and long-term diffusion dynamics [28]. Hydrophobic matrices often exhibit weak interactions with hydrophilic drugs, leading to surface-localized drug aggregation and rapid depletion upon immersion [29]. Moreover, prolonged immersion causes fiber swelling and fusion, channeling drug diffusion toward scaffold peripheries and further disrupting controlled release kinetics. To mitigate these limitations, surface coatings using poly-L-lysine (PLL) or gelatin have been used to enhance cell adhesion and scaffold hydrophilicity [30]. However, such treatments involve multistep processing and often lack stability under physiological conditions [31,32]. In contrast to conventional surface modifications, our previous research employed a copolymerization strategy by incorporating L-lysine moiety onto PBG backbones, achieving intrinsic enhancements in scaffold hydrophilicity and cellular compatibility. However, prior studies typically incorporated L-lysine at low concentration ratios, which proved insufficient to fully resolve the hydrophobicity issue and, in some cases, compromised mechanical strength or disrupted fiber morphology [33]. Additionally, electrospun drug delivery systems based on PLGA (poly(lactic-*co*-glycolic acid)), PCL (poly-ε-caprolactone), or unmodified PBG often exhibited an initial burst release within the first 8–12 h and rarely supported high MH loading levels (>4 wt%) without inducing cytotoxic effects due to uncontrolled drug leaching. These limitations underscore the need for a more integrated material design that simultaneously enhances scaffold hydrophilicity, preserves structural integrity, and enables stable high-capacity drug encapsulation.

In this study, we systematically explored a series of N-ε-carbobenzoxy-L-lysine (CBZL) and γ-benzyl-L-glutamate (BG) copolymer compositions to identify an optimal balance between lysine content and electrospun fibrous scaffold properties. Among these, a 7:3 CBZL:BG ratio emerged as the most promising candidate, offering high lysine incorporation to intrinsically enhance scaffold hydrophilicity and cellular compatibility, while maintaining favorable fiber morphology and mechanical integrity. This optimized copolymer enabled the stable encapsulation of up to 6 wt% MH without compromising cell viability, facilitated by improved polymer-drug interactions and a tri-phasic drug release profile. We comprehensively characterized the physicochemical properties of these scaffolds, analyzed drug release kinetics, and assessed their effects on neuronal cell viability and neurite outgrowth. The 7:3 copolymer scaffold significantly promoted neurite extension, achieving an average length of 214 μm compared to 143 μm in controls. This bifunctional platform, featuring a hydrophilic, cell-supportive matrix and sustained neuroprotective drug delivery, presents a compelling strategy for CNS repair, addressing persistent challenges in scaffold design, drug loading stability, and bio-functionality in neural tissue engineering.

2. 2. Experimental procedure

2.1. Chemicals, reagents and materials

All chemicals used for polymer synthesis and scaffold fabrication were of analytical grade and used as received unless otherwise specified. The monomers γ-benzyl-L-glutamate (BG) and N-ε-carbobenzyloxy-L-lysine (CBZL), as well as triphosgene and sodium metal, were purchased from Sigma-Aldrich. Organic solvents, including tetrahydrofuran (THF), dimethylformamide (DMF), and dimethylacetamide (DMAc), were obtained from commercial sources and dried as needed. Minocycline hydrochloride (MH, ≥98%) was acquired from (TCI, Japan). For cell culture, RPMI-1640 medium (Gibco, USA), fetal bovine serum (Gibco, USA), horse serum (Gibco, USA), nerve growth factor (Sigma-Aldrich, USA), penicillin–streptomycin (Gibco, USA), and phosphate-buffered saline (Gibco, USA) were purchased from commercial suppliers. Standard reagents used for cell staining and viability assays included Alamar Blue (Invitrogen, USA), Live/Dead Viability/Cytotoxicity Kit (Invitrogen, USA), 4′,6-diamidino-2-phenylindole (DAPI, Invitrogen, USA), phalloidin-TRITC (Sigma-Aldrich, USA), and Bovine Serum Albumin (BSA, Sigma-Aldrich, USA). Throughout this study, the following nomenclature is adopted: poly(γ-benzyl-L-glutamate) as PBG; poly(N-ε-carbobenzoxy-L-lysine) as PCBZL; γ-benzyl-L-glutamate N-carboxyanhydride as BG-NCA, N-ε-carbobenzoxy-L-lysine-N-carboxyanhydride as CBZL-NCA; and the copolymer poly($(CBZL)_m$-*co*-$(BG)_n$), as P($(CBZL)_m$-co-$(BG)_n$), where specific molar ratios (e.g., m:*n* = 7:3, 7CBZL3BG) denote the composition.

The procedures for the synthesis and characterization of copolymers are described in supporting information.

2.2. Fabrication and characterization of scaffold

Electrospun nanofiber scaffolds were fabricated using a series of synthesized P($(CBZL)_m$-co-$(BG)_n$) copolymers with varying molar ratios of CBZL to BG, including 1:0, 3:7, 5:5, 7:3, and 0:1 compositions. Among these, the 7:3 ratio (referred to as 7CBZL3BG) was selected for subsequent drug release and biological evaluations due to its superior balance of hydrophilicity, processability, and mechanical integrity. The copolymers were dissolved in a binary solvent system of DMAc:acetone (1:2 *v*/v) with MH at concentrations of 2, 4, 6, or 8 wt%. The solutions were stirred overnight at room temperature to ensure complete dissolution. Electrospinning (FALCO 300, Hong Zhun, Taiwan) was performed under ambient conditions (50–60% relative humidity) using a syringe pump with a 21-gauge needle and a high-voltage power supply. A high-voltage power supply was applied to generate aligned fibers on a rotating drum wrapped with baking paper. Fiber mats were collected over 20 min for drug release studies. For cell culture experiments, fibers were deposited directly onto 12 mm glass coverslips affixed to aluminum foil on the collector, using a 1.5 min electrospinning time. The scaffolds were then transferred to 24-well plates for subsequent cell seeding. **Table S1** lists the electrospinning parameters, including polymer concentration, applied voltage, flow rate, and drum rotation speed.

2.3. Measurement and kinetic study of drug release

Drug release from electrospun scaffolds was evaluated in phosphate-buffered saline (PBS, pH = 7.4) at 37 °C. In vitro drug release studies were performed using a thermal water bath (FIRSTEK RB-120, Taiwan). Each scaffold (10.6 mg) was immersed in 24 mL PBS with gentle shaking. At designated time points (2 to 35 h), 2 mL of the release medium was collected each time and then replenished with fresh PBS at 37 °C. The MH concentration in the copolymer scaffold was determined by UV–Vis spectrophotometer at λ = 265 nm (V-700, JASCO, Japan). To determine total drug loading, scaffolds were dissolved in DMF and measured as 100% release reference, as shown in **Fig. S1**. Cumulative release was calculated as:

$$\textit{Cumulative release}\ (\%) = \frac{\text{weight of the drug releasd}}{\text{weight of the total drug}} \times 100$$

Drug release profiles were quantified using the UV–Vis method described above. All release experiments were performed in triplicate, and the data are presented as mean ± standard deviation (SD) ($n = 3$).

To better understand the drug release mechanism, the cumulative

release data were divided into three distinct phases based on slope transitions and fitted using various kinetic models: zero-order, first-order, Higuchi, Ritger–Peppas, and Weibull equations. Curve fitting employed both linear and nonlinear regression methods depending on the model requirements. The general cumulative release percentage at time t is defined as:

$$Q_t = \frac{M_t}{M_\infty} \times 100\%$$

where M_t is the cumulative amount of drug released at time t, and M_∞ is the total amount of drug released at equilibrium. The zero-order kinetic model follows the equation $Q_t = Q_0 + k(t - t_0)$, indicating a constant release rate over time. The first-order model is expressed as $Q_t = Q_0 + \left(1 - e^{-k(t-t_0)}\right)$, which assumes the release rate is proportional to the remaining drug loading. The Higuchi model, given by $Q_t = Q_0 + k(t - t_0)^{\frac{1}{2}}$, is based on Fickian diffusion and is typically applied to matrix-based drug release systems. In all three models, Q_0 and t_0 are fitting constants to account for non-zero initial conditions, such as when fitting begins in later phases (phase II or III). The Ritger-Peppas equation is described by the power-law equation $Q_t = kt^n$, where the exponent n characterizes the drug release mechanism. Specifically, if $n < 0.45$, the release follows Fickian diffusion; if $n > 0.89$, matrix relaxation or erosion dominates the release process; and for values of n between 0.45 and 0.89, a non-Fickian or anomalous transport mechanism is implied, involving a combination of diffusion and polymer matrix relaxation. The Weibull Equation is expressed as $F(t) = 1\text{-}\exp\left[-\left(\frac{t-T_i}{\alpha}\right)^{\beta}\right]$, where T_i, α, and β are model parameters. This model is particularly suitable for describing complex, non-linear, or multi-mechanistic drug release behaviors in advanced biomaterials such as electrospun fibers, hydrogels, or core–shell systems. Its high flexibility enables it to accurately describe release profiles that deviate from classical kinetic models, thereby offering more comprehensive insight into the influence of material properties and drug distribution on the overall release kinetics.

2.4. Cell culture

PC-12 cells (BCRC, Taiwan) were cultured in RPMI-1640 medium supplemented with 10% horse serum, 5% fetal bovine serum, and 1% penicillin–streptomycin. Cells were seeded onto 24-well plates (Simply Biologics, Taiwan) containing 12 mm glass coverslips at a density of 1×10^4 cells/well. For differentiation, 100 ng/mL nerve growth factor (NGF, Sigma-Aldrich, USA) was added to the culture medium. Cells were cultured in a CO_2 incubator (MCO-239AICUVL-PA, PHCbi, PHC Corporation, Tokyo, Japan) at 37 °C in a humidified atmosphere with 5% CO_2.

2.5. Statistical analysis

All investigations were performed in triplicate, and the results are presented as mean ± standard deviation. Statistical differences between groups were determined using one-way analysis of variance (ANOVA) with Microsoft Excel, and a significance level of $p < 0.05$ was considered statistically significant. Neurite lengths were quantified using the integrated digital measurement suite of the ECHO Revolve hybrid microscope system. To ensure data reliability and statistical representativeness, measurements were performed on randomly selected cells across multiple fields of view, with a consistent sample size of $n = 15$ per experimental group.

3. Results and discussion

To investigate the influence of polymer composition on scaffold performance, we synthesized a series of polypeptide-based copolymers via NCA ring-opening polymerization using sodium methanolate as an initiator (Fig. 1a). Three different feed ratios of lysine to glutamic acid (3:7, 5:5, and 7:3) were employed to modulate the hydrophilicity and interfacial properties of the resulting copolymers. GPC analysis confirmed that the molecular weights of all synthesized copolymers were well-controlled within the range of 700–800 kDa, with narrow dispersity (PDI < 1.5), ensuring the formation of robust nanofibers suitable for electrospinning, as shown in Fig. S2. FTIR spectroscopy further verified the successful polymerization and chemical composition of the materials. The presence of characteristic peaks, including 3287 cm^{-1} (N—H stretching), 2920 cm^{-1} (C—H stretching), 1734 cm^{-1} (C═O ester), 1650 cm^{-1} (amide I, N–HC═O), and 1543 cm^{-1} (amide II, N–HC═O), confirmed the incorporation of both glutamate and lysine-derived residues into the polymer backbone (Fig. 1b). Peaks associated with the CBZL and benzyl protecting groups, such as 1245 cm^{-1} (CBZ, C—O), 1165 cm^{-1} (Bn, C—O), and 745 and 698 cm^{-1} (phenyl), were also observed, indicating the presence of side-chain functionalities that are essential for hydrophilic tuning and subsequent drug interactions. Furthermore, ^{1}H NMR spectra (Fig. S3) provided additional confirmation of the chemical structure of P((CBZL)m-co-(BG)n). The characteristic chemical shifts (δ) were assigned as follows: 7.50 ppm (a; Ar—H), 5.37 ppm (b; CH_2-benzylic), 4.96 ppm (c; C—H, amide of glutamate), 4.76 ppm (c″; C—H, amide of lysine), 3.37 ppm (d; γ-CH_2 of glutamate), 2.73 ppm (e; ε-CH_2 of lysine), 2.22 ppm (f; β-CH_2), and 1.47 ppm (g; γ, δ-CH_2). These signals are consistent with the expected structural units of glutamate and lysine within the copolymer, further confirming the successful copolymerization and composition of the materials. These results demonstrate that the copolymer composition can be precisely controlled via tunning the molecular architecture, laying the foundation for structure-property relationships explored in subsequent sections.

To optimize scaffold diameter for neural tissue regeneration, electrospun fibrous networks were fabricated using copolymers with various lysine content (3CBZL7BG, 5CBZL5BG, and 7CBZL3BG). As shown in the SEM photos of fibrous scaffolds (Fig. 2a–c), all three scaffolds formed continuous, oriented fibers with diameters near 0.8–0.9 μm, closely mimicking the native axonal environment [33]. This structural similarity is considered critical for promoting axon guidance, cell adhesion, and neurite outgrowth. Surface hydrophilicity was subsequently evaluated to determine the impact of lysine content on scaffold hydrophilicity. Water contact angle measurements (Fig. 2d) revealed a clear trend: contact angles decreased from 122.6° ± 4.9° (PBG) to 103.2° ± 3.6° (3CBZL7BG) to 96.3° ± 1.5° (5CBZL5BG) and further to 83.6° ± 4.9° (7CBZL3BG), indicating progressively enhanced hydrophilicity with increasing lysine content. This improvement is attributed to the amide bonds in CBZL that enhance hydrophilicity through hydrogen bond formation with water molecules. The 7CBZL3BG scaffold, which exhibited the lowest contact angle, was thus selected as the model system for subsequent drug loading and release studies due to its superior water compatibility and favorable surface properties for neuronal cell interaction.

The mechanical properties of the scaffolds are summarized in Table 1 with increasing lysine content, the intermolecular hydrogen bonding between polymer chains is reduced, leading to weakened chain–chain interactions. This reduction results in a decrease in Young's modulus and a significant increase in material deformability, as evidenced by the enhanced elongation at break. Notably, the 7CBZL3BG scaffold exhibited an elongation of 57.1%, indicating a highly flexible and compliant structure. Such mechanical characteristics are particularly important for neural regeneration, where soft and elastic substrates are required to support cell attachment and accommodate dynamic neurite extension. Therefore, the 7CBZL3BG scaffold, with its improved flexibility and suitable mechanical properties, is considered highly favorable for neural tissue engineering applications.

To evaluate the influence of drug loading on scaffold morphology, MH was incorporated into the 7CBZL3BG scaffold at concentrations of 2, 4, 6, and 8 wt%. As depicted in Fig. 3a–d, electrospun fibers maintained

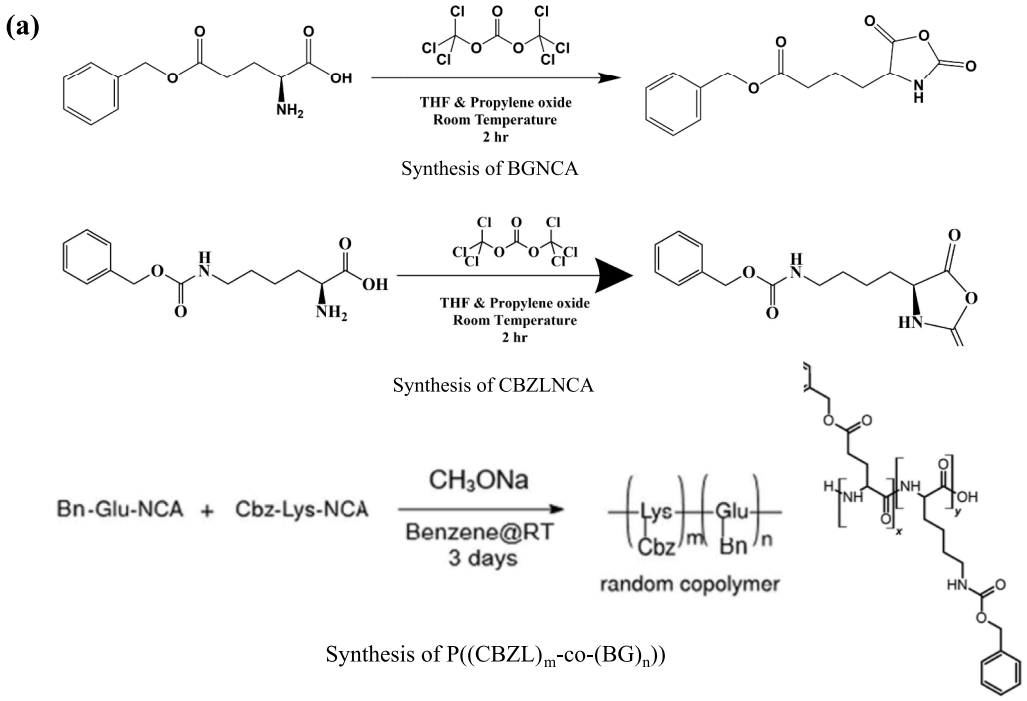

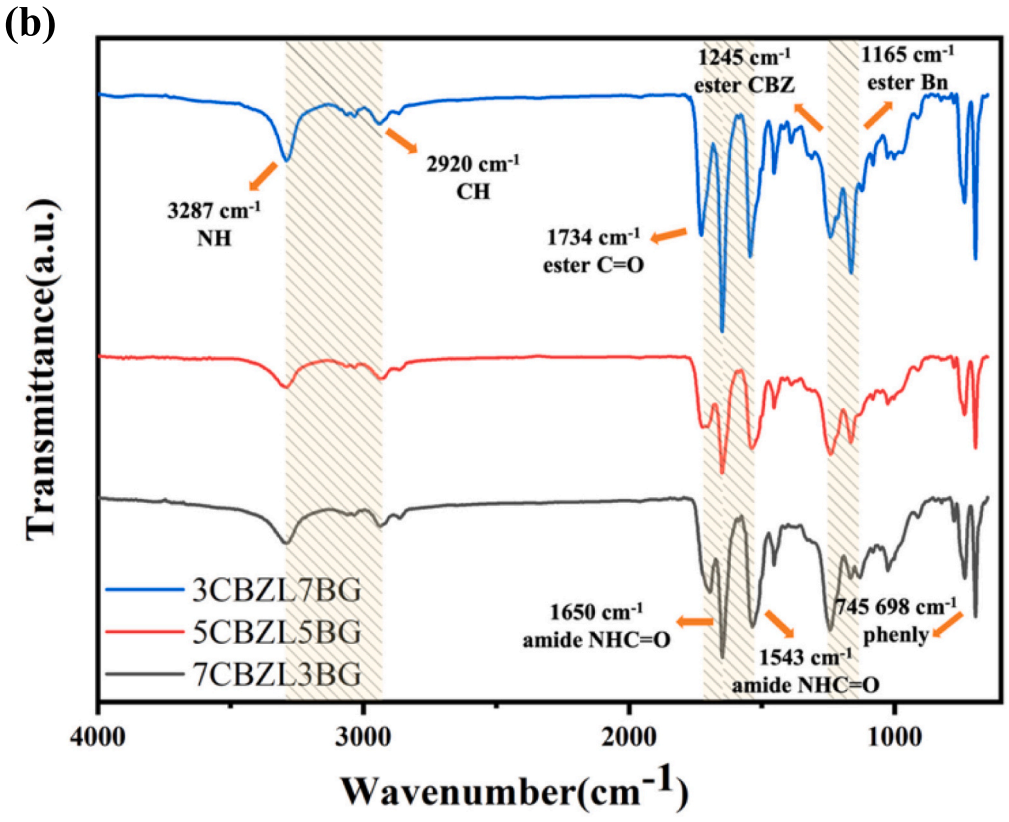

Fig. 1. (a) Chemical reaction of the polymerization. (b) ATR-FTIR penetration spectra of P((CBZL)$_m$-co-(BG)$_n$).

a uniform and interconnected architecture across all formulations. Notably, fiber diameters exhibited a concentration-dependent reduction with increasing minocycline loading: the average diameter decreased from 0.84 ± 0.14 μm (2 wt%) to 0.78 ± 0.16 μm (4 wt%) and 0.77 ± 0.19 μm (6 wt%) and further to 0.76 ± 0.10 μm (8 wt%). The observed thinning effect is likely due to enhanced solution conductivity induced by MH, which increases electrostatic stretching forces during electrospinning and facilitates finer fiber formation. In addition to reducing fiber diameter, MH also improved morphological uniformity, resulting in narrower diameter distributions and more consistent microstructure.

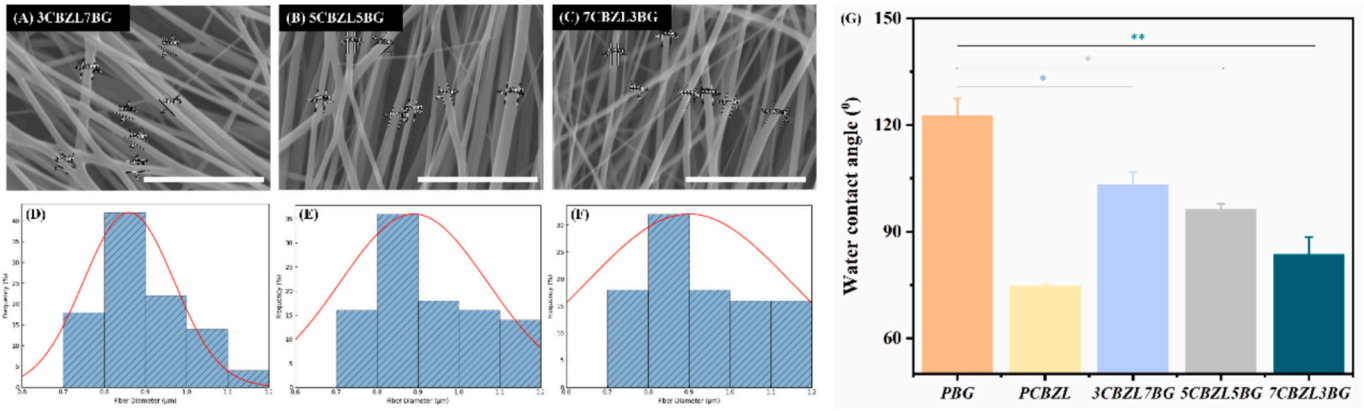

Fig. 2. SEM images of electrospun P((CBZL)m-co-(BG)n) scaffolds: (a) 3CBZL7BG, (b) 5CBZL5BG, and (c) 7CBZL3BG. (d–f) Corresponding fiber diameter distribution histograms of (a–c), respectively. The fiber diameters were measured from randomly selected fibers for each sample ($n = 50$). Scale bars = 10 μm. (g) Water contact angles of the scaffolds (mean ± SD, $n = 3$ independent samples). *$p < 0.05$, **$p < 0.01$, ***$p < 0.001$.

Table 1
Mechanical properties of copolymer scaffolds with different CBZL/BG ratios, including Young's modulus, breaking force, and elongation at break.

Polymer	Young's modulus (MPa)	Breaking force (gf)	Elongation (%)
3CBZL7BG	55.0 ± 3.5	1593.2 ± 33.1	7.0 ± 1.1
5CBZL5BG	37.4 ± 0.6	484.8 ± 41.3	13.1 ± 1.2
7CBZL3BG	7.6 ± 0.2	330.9 ± 43.3	57.1 ± 13.1

These improvements are critical for drug delivery applications: uniform fiber networks support more homogeneous drug encapsulation, reduce localized burst release, and offer tighter control over diffusion pathways. Collectively, the enhanced structural homogeneity and nanoscale fiber tuning achieved through MH incorporation are expected to improve the stability and reproducibility of drug release profiles, offering a tunable platform for long-term neuroprotective delivery.

To examine the effect of MH concentration on release kinetics, cumulative drug release was quantified from 7CBZL3BG scaffolds loaded with 2, 4, 6, and 8 wt% MH. As shown in Fig. 3e, the 2 wt% group exhibited a pronounced initial burst within the first 48 h, followed by a plateau, indicative of rapid drug depletion. In contrast, the 6 wt% group demonstrated a markedly slower and more sustained release over 14 days. This sustained profile is associated with increased drug-polymer interactions at higher loading levels, which limit premature release and enhance matrix retention. The intermediate 4 wt% formulation displayed a balanced profile between the two extremes. Further analysis of the early-stage kinetics (Fig. 3f) reveals that low-concentration scaffolds are more susceptible to swelling-induced channel formation, which accelerates drug diffusion, while higher drug loading appears to stabilize the polymer network against such effects. These data support the hypothesis that increasing minocycline concentration shifts the release behavior from a swelling-dominated burst mechanism toward a more diffusion-controlled process. In addition, from the perspective of drug–polymer interactions, the hydrophilic nature of minocycline (MH) plays a crucial role in modulating its release behavior. As illustrated in Scheme S1, MH exhibits favorable affinity with the hydrophilic 7CBZL3BG copolymer matrix via specific hydrogen bonding. This strong interfacial interaction prevents macroscopic phase separation during electrospinning, ensuring a high loading capacity. Furthermore, it leads to a more homogeneous distribution within the fibrous network. This improved compatibility reduces localized drug aggregation and suppresses the initial burst release. Furthermore, the hydrophilic matrix facilitates water penetration and scaffold swelling, promoting gradual diffusion of the drug from the interior to the surface, thereby enabling a more sustained and controlled release profile.

To elucidate the underlying mechanisms governing drug release, cumulative minocycline (MH) release profiles were quantitatively analyzed using established kinetic models, including first-order, Korsmeyer–Peppas, and Weibull functions. As shown in Fig. 4a, the 2 wt% MH group exhibited the best fit to a first-order release model (R^2 = 0.944), indicating a concentration-dependent mechanism likely driven by rapid water uptake and swelling of the hydrophilic copolymer matrix at low drug loadings. This swelling-enhanced release deviated from typical Fickian diffusion behavior, especially during the early phase, consistent with previous observations for low-density electrospun systems. In contrast, formulations containing 4 wt% and 6 wt% MH showed higher correlation with the Korsmeyer–Peppas model (R^2 = 0.962 and 0.977, respectively), with diffusional exponents (n-values) between 0.43 and 0.51, as shown in Fig. 4b. These results reflect a predominantly Fickian diffusion mechanism, where drug release is sustained by a persistent concentration gradient without significant matrix swelling or erosion. This behavior aligns with the intermediate hydrophilicity and stable fiber morphology observed in the 7CBZL3BG scaffolds at these drug loadings. "Beyond surface wettability, the enhanced hydrophilicity of the lysine-functionalized copolymer plays a fundamental role in modulating drug distribution and subsequent release kinetics. The increased density of polar functional groups within the 7CBZL3BG matrix facilitates robust hydrogen-bonding interactions and dipole-dipole affinities with the minocycline (MH) molecules. These favorable polymer–drug interactions promote a more homogeneous molecular dispersion within the fibrous network, effectively suppressing the thermodynamic drive for drug migration and aggregation at the fiber surface during the electrospinning process. By ensuring a uniform internal distribution, the matrix effectively mitigates the initial burst release typically caused by surface-localized drug. Furthermore, the hydrophilic nature of the scaffold ensures more uniform water infiltration and controlled polymer swelling, which establishes a stable environment for diffusion-governed release. This synergistic relationship between chemical structure, molecular interaction, and drug distribution provides a comprehensive mechanistic basis for the sustained release profiles observed across varying drug loadings." Interestingly, when the MH concentration was further increased to 8 wt% (MH8), the release profile could no longer be adequately described by either the first-order or Korsmeyer–Peppas model. Instead, it followed a Weibull distribution with a high degree of fit (R^2 = 0.983; Fig. 4c). The calculated shape parameter ($\beta = 0.568$) indicated a biphasic release mechanism involving an initial surface-mediated burst phase, likely due to drug accumulation near the fiber surface, followed by a diffusion-limited phase characterized by reduced gradient strength and diminished release potential. This hybrid mechanism underscores the complexity introduced by excessive drug loading, where polymer–drug interactions and surface saturation begin to dominate over traditional diffusion. The comparative model

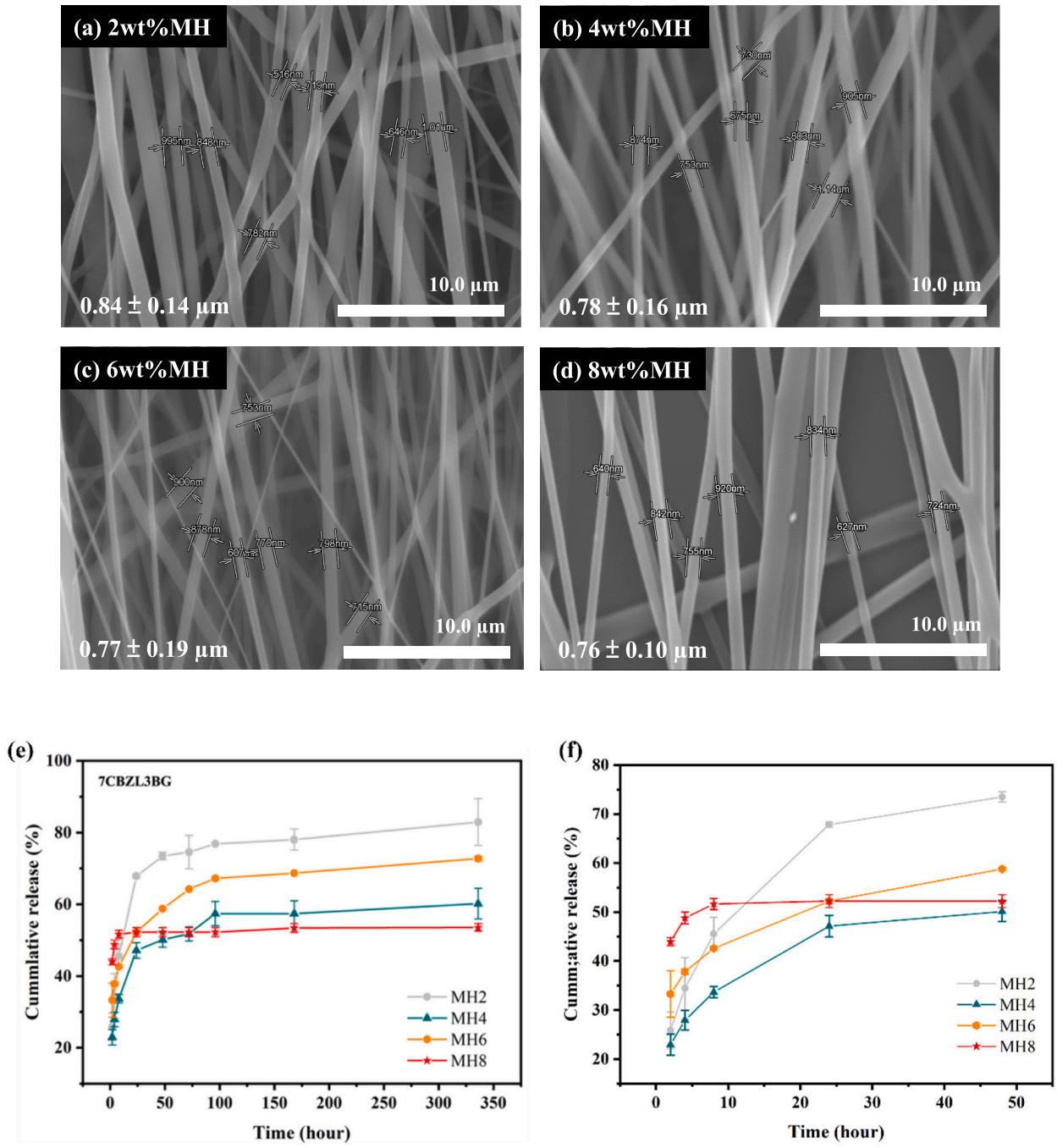

Fig. 3. SEM images of scaffolds loaded with different concentrations of minocycline (MH): (a) 2 wt%, (b) 4 wt%, (c) 6 wt%, and (d) 8 wt%. The fiber diameters were measured from 7 randomly selected fibers for each sample ($n = 7$). Scale bars = 10 μm. (e) Cumulative release profiles of MH-loaded scaffolds at different concentrations (2, 4, 6, and 8 wt%). (f) Early-stage cumulative release (0–48 h) of MH-loaded scaffolds.($n = 3$).

fitting results, as listed in Table 2, collectively demonstrate that drug concentration not only influences release duration but also dictates the governing kinetic pathway: transitioning from first-order release at low concentrations (MH2), to Fickian diffusion at moderate levels (MH4, MH6), and eventually to a Weibull-type hybrid model at higher loadings (MH8). The initial burst release (Phase 1) is primarily a surface-mediated process. In contrast, the secondary stage (Phase 2) is highly sensitive to the CBZL/BG ratio. As the lysine (CBZL) content increases, the reduction in intermolecular hydrogen bonding—evidenced by the increased elongation shown in Table 1—enhances water uptake and promotes matrix expansion. This structural relaxation creates diffusion pathways that facilitate the migration of drug molecules from the fiber core into the surrounding medium. The transition to Phase 3 corresponds to a sustained release regime, governed by the gradual relaxation of the hydrophilic copolymer network. By correlating the Korsmeyer–Peppas n-values with the observed mechanical compliance of the 7CBZL3BG scaffold, we conclude that the release mechanism arises from a synergistic interplay between diffusion and swelling-controlled relaxation. This behavior is uniquely enabled by the tunable intermolecular interactions within the CBZL/BG copolymer system. These findings highlight the critical need to optimize drug loading in electrospun scaffolds to achieve a balance between sustained release, loading capacity, and therapeutic efficacy for CNS repair applications. In addition, we monitored the pH of the release medium over 14 days to explore

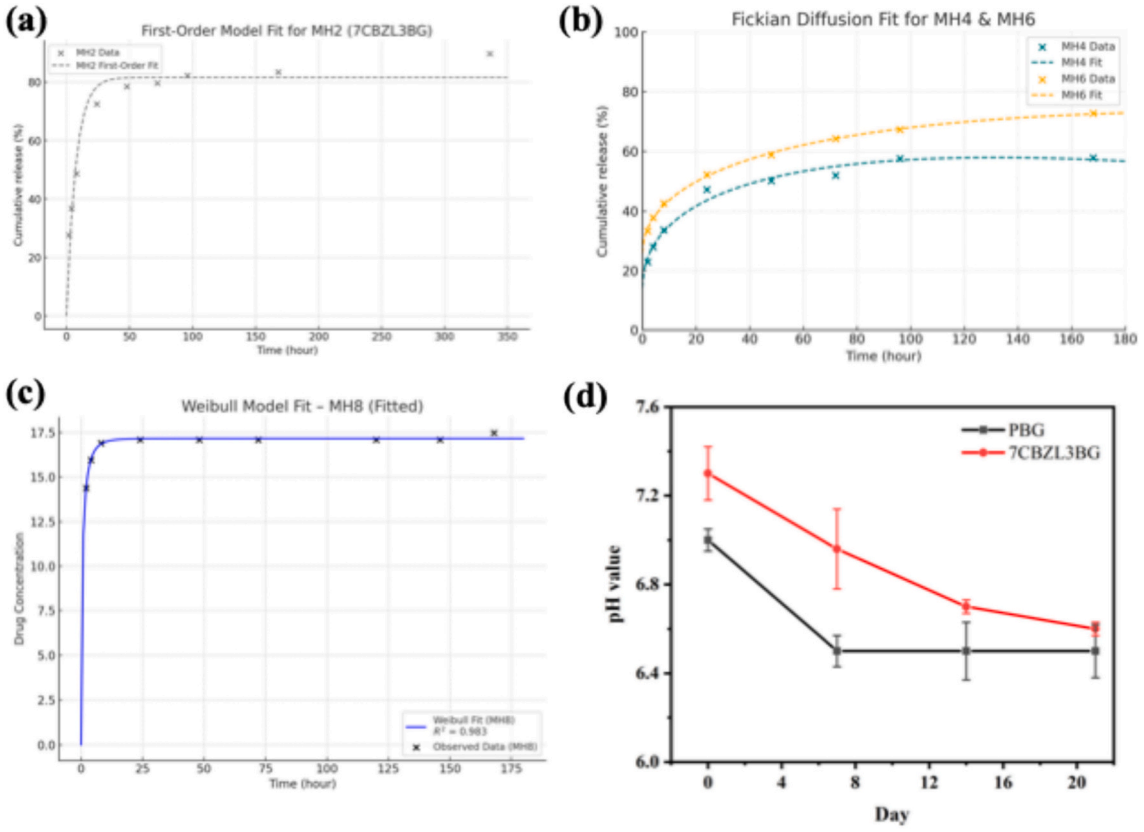

Fig. 4. Model fitting of minocycline release profiles: (a) First-order model (MH2), (b) Fickian diffusion model (MH4 and MH6), (c) Weibull model (MH8), (d) pH variations of culture medium for PBG and copolymer scaffolds over 21 days (n = 3).

Table 2
Comparative analysis of release kinetics models.

MH loading (wt%)	Best-fit model	R^2	n
2	First-order	0.94	–
4	Korsmeyer-Peppas	0.92	0.24
6	Korsmeyer-Peppas	0.97	0.26
8	Korsmeyer-Peppas	0.98	$\beta = 0.568$

potential microenvironmental changes during release. As shown in Fig. 4d, a gradual acidification trend was observed across all drug-loaded scaffolds, with pH values decreasing from 7.4 to approximately 6.8 by day 14. This may reflect early-stage hydrolysis of the glutamate-derived ester side chains within the PBG-based copolymer matrix. While this acidification did not immediately affect release kinetics within the observed period, it may contribute to enhanced drug solubility or scaffold degradation over longer time scales. These results collectively indicate that drug concentration strongly influences the release kinetics, from first-order behavior at low concentrations to Fickian diffusion and eventually Weibull-type hybrid kinetics at higher loadings. The pH trend further highlights the importance of considering polymer microenvironment evolution when designing controlled release systems for long-term neurotherapeutic delivery.

To assess the biological relevance of the release behavior, in vitro cytocompatibility tests were conducted using PC-12 cells cultured on drug-loaded scaffolds. As shown in Fig. 5a, cell viability increased significantly with MH loading up to 6 wt%, consistent with the known neuroprotective and anti-inflammatory effects of the drug. Notably, the 6 wt% group exhibited the highest density of viable cells and the lowest level of cytotoxicity, indicating an optimal concentration range for therapeutic benefit. However, at 8 wt% MH loading, a marked decline in viability was observed (Fig. 5b), likely due to excessive local drug concentrations exceeding the cytotoxic threshold. This dose-dependent effect highlights a narrow therapeutic window for minocycline delivery and underscores the importance of tuning drug loading to avoid off-target toxicity. In contrast, cells cultured on traditional PBG scaffolds with equivalent minocycline content showed greater cytotoxicity, attributed to uncontrolled burst release during the early phase. A quantitative summary (Fig. 5c) of live/dead cell ratios confirms that the 7CBZL3BG system with 6 wt% MH achieves the most favorable outcome in terms of both biocompatibility and therapeutic efficacy. These results suggest the dual-functional role of the copolymer scaffold in mitigating early cytotoxicity and supporting long-term neuroprotection.

To further evaluate the neurodegenerative potential of the 7CBZL3BG scaffolds, the effect of sustained MH release on neurite outgrowth was investigated using differentiated PC-12 cells. As shown in Fig. 6, MH incorporation induced a concentration-dependent enhancement in neurite extension. In the absence of MH (Fig. 6a), neurite lengths remained limited (<90 μm), consistent with the passive support capacity of the scaffolds. Upon loading 2 wt% MH (Fig. 6b), a modest but statistically significant increase in neurite length was observed, indicating that even low-dose delivery could promote early-stage neuronal differentiation. The effect was further amplified at 4 wt% (Fig. 6c), while the most pronounced elongation occurred at 6 wt% (Fig. 6d), with average neurite lengths extending up to 214 μm. At this concentration, neurites appeared long, continuous, and well-aligned across the fibrous scaffold surface, suggesting that sustained exposure to MH created a pro-regenerative microenvironment conducive to axonal guidance. Interestingly, although neurite length remained elevated at 8 wt% MH, both the maximum and minimum lengths exhibited greater variability, and some neurites appeared fragmented or misoriented, as presented in Fig. 6e. This reduction in structural uniformity suggests that local MH oversaturation, even under sustained-release conditions, may subtly disrupt the biochemical signaling

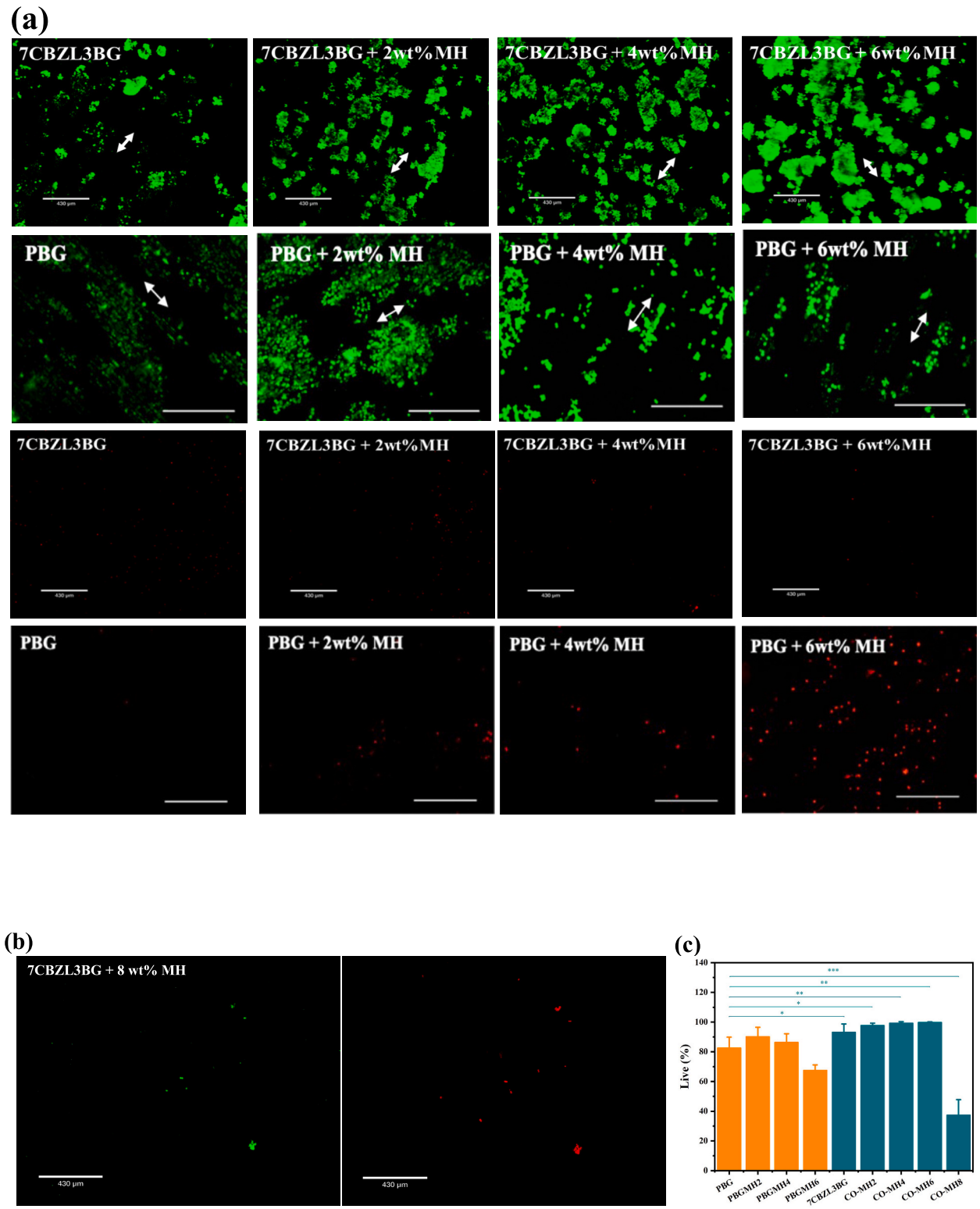

Fig. 5. (a) Live/Dead staining of PC12 cells cultured on scaffolds with different MH loadings. Green indicates live cells (calcein-AM), and red indicates dead cells (PI). (b) Increasing MH concentration (≥8 wt%) resulted in reduced cell viability. (c) Quantitative analysis of PC12 cell viability on PBG- and 7CBZL3BG-based scaffolds with varying MH concentrations ($n = 4$). Data are presented as mean ± standard deviation. Statistical significance was determined between groups, with $*p < 0.05$, $**p < 0.01$, and $*p < 0.001$.

balance essential for consistent neurite maturation. Box plot analysis (Fig. 6f) quantitatively confirmed these observations: the median neurite lengths were 88.4 μm (0 wt% MH), 91.6 μm (2 wt% MH), 102.5 μm (4 wt% MH), 214 μm (6 wt% MH), and 183 μm (8 wt% MH). Compared to traditional PBG scaffolds, the 7CBZL3BG system consistently outperformed in both maximum neurite length and distribution homogeneity, reinforcing the role of the lysine-modified copolymer in enhancing differentiation through both structural and pharmacological mechanisms. Collectively, these findings demonstrate that the 7CBZL3BG scaffold, when loaded with an optimal concentration of

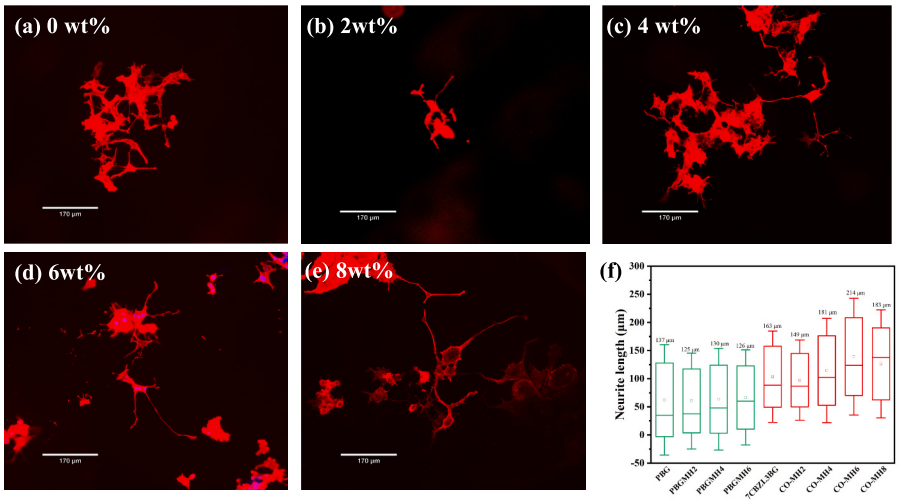

Fig. 6. Immunofluorescence images of PC-12 cells cultured on 7CBZL3BG scaffolds with different MH concentrations: (a) 0 wt%, (b) 2 wt%, (c) 4 wt%, (d) 6 wt%, and (e) 8 wt%. (f) Quantitative analysis of neurite length of PC-12 cells cultured on PBG and 7CBZL3BG scaffolds with varying MH concentrations. Neurite lengths were measured from 15 randomly selected cells ($n = 15$) using the built-in measurement function of a cell imaging system (ECHO Revolve, ECHO Laboratories, USA).

minocycline, not only supports cell survival but also actively promotes neurite length, a key prerequisite for successful neural repair. The dual-mode function of this system, combining sustained therapeutic release with topographical and biochemical cues, positions it as a compelling platform for advanced neural tissue engineering. Furthermore, to benchmark the neural regenerative potential of this optimized environment, a horizontal comparison with previously reported nerve scaffolds was conducted **(Table S2)**. The comparison explicitly demonstrates that our optimal 7CBZL3BGMH6 scaffold achieves superior neurite outgrowth (123 μm) relying entirely on its intrinsic bioactivity and sustained drug delivery. Unlike conventional systems that require complex post-electrospinning surface coatings (e.g., polylysine or laminin) or external stimulation, our scaffold promotes robust neurite extension solely through its molecular design. This confirms that the developed copolymer matrix provides a more robust, multifunctional, and streamlined platform for neural tissue engineering.

4. Conclusion

In this study, we synthesized the copolymer P((CBZL)$_m$-*co*-(BG)$_n$) via ring-opening anionic polymerization of γ-benzyl-L-glutamate and N-carbobenzoxy-L-lysine. This lysine-functionalized copolymer offers a unique advantage over conventional PBG materials by eliminating the need for polylysine surface coating in cell culture, thereby simplifying experimental procedures, minimizing variability, and reducing potential handling errors. The incorporation of lysine moiety in the chemical structure of PBG bachbond not only enhanced the hydrophilicity of the copolymer, but also significantly improved its bioactivity, overcoming the poor cell adhesion commonly associated with pristine PBG while retaining the glutamate-mediated promotion of neural growth and differentiation. Among the compositions tested, the 7:3 CBZL:BG copolymer (7CBZL3BG) exhibited optimal surface hydrophilicity and structural integrity, supporting superior neural cell adhesion and viability. Moreover, this scaffold demonstrated a significantly enhanced drug-loading capacity, accommodating up to 6 wt% MH without inducing cytotoxicity. Compared to unmodified PBG-based systems, the 7CBZL3BG scaffold effectively supported sustained MH delivery and improved neurite outgrowth, with average neurite lengths extending from 143 μm in controls to 214 μm. These results highlight the scaffold's dual functionality, facilitating both cell adhesion and therapeutic delivery, without the need for additional surface modification or pre-treatment. Importantly, the copolymer matrix enabled controlled MH release across a range of drug concentrations, with a significantly reduced initial burst and minimized burst-related cytotoxicity while sustaining neuroprotective efficacy. This stable release behavior, coupled with intrinsic cell-adhesive properties, underscores the potential of lysine-functionalized copolymers as a versatile platform for neural tissue engineering and drug delivery applications.

CRediT authorship contribution statement

Yu-Ting Lin: Writing – original draft, Visualization, Validation, Methodology, Investigation, Formal analysis, Data curation. **Wei-Fang Su:** Writing – review & editing, Conceptualization. **Yu-Sheng Hsiao:** Supervision, Funding acquisition. **Chun-Yu Chang:** Investigation. **Meng-Fang Lin:** Supervision, Resources, Investigation, Funding acquisition. **Yu-Ching Huang:** Writing – review & editing, Supervision, Project administration, Funding acquisition, Conceptualization.

Declaration of competing interest

The authors declare the following financial interests/personal relationships which may be considered as potential competing interests: Yu-Ching Huang reports financial support was provided by National Science and Technology Council of Taiwan. If there are other authors, they declare that they have no known competing financial interests or personal relationships that could have appeared to influence the work reported in this paper.

Acknowledgments

This research was supported in full by the National Science and Technology Council of Taiwan (Grant numbers: NSTC 114-2221-E-131-012-MY3, 114-2628-E-011-003-MY3, 114-2221-E-131-038, 112-2628-E-131-001-MY4).

Appendix A. Supplementary data

Supplementary data to this article can be found online at https://doi.org/10.1016/j.surfcoat.2026.133610.

Data availability

Data will be made available on request.

References

[1] B.S. Mietto, K. Mostacada, A.M. Martinez, Neurotrauma and inflammation: CNS and PNS responses, Mediat. Inflamm. 2015 (2015) 251204, https://doi.org/10.1155/2015/251204 From NLM.

[2] J.D. Houle, M.P. Côté, Axon regeneration and exercise-dependent plasticity after spinal cord injury, Ann. N. Y. Acad. Sci. 1279 (1) (2013) 154–163, https://doi.org/10.1111/nyas.12052 From NLM.

[3] P. Teotia, M.J. Van Hook, D. Fischer, I. Ahmad, Human retinal ganglion cell axon regeneration by recapitulating developmental mechanisms: effects of recruitment of the mTOR pathway, Development 146 (13) (2019), https://doi.org/10.1242/dev.178012. From NLM.

[4] R. Boni, A. Ali, A. Shavandi, A.N. Clarkson, Current and novel polymeric biomaterials for neural tissue engineering, J. Biomed. Sci. 25 (1) (2018) 90, https://doi.org/10.1186/s12929-018-0491-8.

[5] P.G. De Deyne, S.M. Kladakis, Bioscaffolds in Tissue Engineering: A Rationale for Use in the Reconstruction of Musculoskeletal Soft Tissues, Clin. Podiatr. Med. Surg. 22 (4) (2005) 521–532, https://doi.org/10.1016/j.cpm.2005.07.006.

[6] A. Subramanian, U.M. Krishnan, S. Sethuraman, Development of biomaterial scaffold for nerve tissue engineering: biomaterial mediated neural regeneration, J. Biomed. Sci. 16 (1) (2009) 108, https://doi.org/10.1186/1423-0127-16-108 From NLM.

[7] G. Perale, F. Rossi, E. Sundstrom, S. Bacchiega, M. Masi, G. Forloni, P. Veglianese, Hydrogels in spinal cord injury repair strategies, ACS Chem. Neurosci. 2 (7) (2011) 336–345, https://doi.org/10.1021/cn200030w From NLM.

[8] C.D.L. Johnson, J.M. Zuidema, K.R. Kearns, A.B. Maguire, G.P. Desmond, D. M. Thompson, R.J. Gilbert, The effect of electrospun fiber diameter on astrocyte-mediated neurite guidance and protection, ACS Appl. Bio Mater. 2 (1) (2019) 104–117, https://doi.org/10.1021/acsabm.8b00432 From NLM.

[9] J.-P. Benoit, N. Faisant, M.-C. Venier-Julienne, P. Menei, Development of microspheres for neurological disorders: From basics to clinical applications, J. Control. Release 65 (1) (2000) 285–296, https://doi.org/10.1016/S0168-3659(99)00250-3.

[10] P. Dubový, I. Klusáková, I. Hradilová Svíženská, Inflammatory Profiling of Schwann Cells in Contact with Growing Axons Distal to Nerve Injury, Biomed. Res. Int. 2014 (1) (2014) 691041, https://doi.org/10.1155/2014/691041.

[11] M. Mota, V. Porrini, E. Parrella, M. Benarese, A. Bellucci, S. Rhein, M. Schwaninger, M. Pizzi, Neuroprotective epi-drugs quench the inflammatory response and microglial/macrophage activation in a mouse model of permanent brain ischemia, J. Neuroinflammation 17 (1) (2020) 361, https://doi.org/10.1186/s12974-020-02028-4.

[12] K. Hashimoto, T. Ishima, A novel target of action of minocycline in NGF-induced neurite outgrowth in PC12 cells: translation initiation [corrected] factor eIF4AI, PLoS One 5 (11) (2010) e15430, https://doi.org/10.1371/journal.pone.0015430.

[13] J.A. Sierra-Fonseca, O. Najera, J. Martinez-Jurado, E.M. Walker, A. Varela-Ramirez, A.M. Khan, M. Miranda, N.S. Lamango, S. Roychowdhury, Nerve growth factor induces neurite outgrowth of PC12 cells by promoting Gβγ-microtubule interaction, BMC Neurosci. 15 (1) (2014) 132, https://doi.org/10.1186/s12868-014-0132-4.

[14] H. Macdonald, R.G. Kelly, E.S. Allen, J.F. Noble, L.A. Kanegis, Pharmacokinetic studies on minocycline in man, Clin. Pharmacol. Ther. 14 (5) (1973) 852–861, https://doi.org/10.1002/cpt1973145852.

[15] A. Mansour, M. Romani, A.B. Acharya, B. Rahman, E. Verron, Z. Badran, Drug delivery systems in regenerative medicine: an updated review, Pharmaceutics 15 (2) (2023), https://doi.org/10.3390/pharmaceutics15020695. From NLM.

[16] H. Nojehdehyan, F. Moztarzadeh, H. Baharvand, H. Nazarian, M. Tahriri, Preparation and surface characterization of poly-L-lysine-coated PLGA microsphere scaffolds containing retinoic acid for nerve tissue engineering: In vitro study, Colloids Surf. B: Biointerfaces 73 (2009) 23–29, https://doi.org/10.1016/j.colsurfb.2009.04.029.

[17] R.B. Shultz, Y. Zhong, Hydrogel-based local drug delivery strategies for spinal cord repair, Neural Regen. Res. 16 (2) (2021), https://doi.org/10.4103/1673-5374.290882.

[18] M. Asadian, K.V. Chan, M. Norouzi, S. Grande, P. Cools, R. Morent, N. De Geyter, Fabrication and plasma modification of nanofibrous tissue engineering scaffolds, Nanomaterials (Basel) 10 (1) (2020), https://doi.org/10.3390/nano10010119. From NLM.

[19] S. Karimi Afshar, M. Abdorashidi, F.A. Dorkoosh, H. Akbari Javar, Electrospun Fibers: Versatile Approaches for Controlled Release Applications, International Journal of Polymer Science 2022 (1) (2022) 9116168, https://doi.org/10.1155/2022/9116168.

[20] E.J. Torres-Martinez, J.M. Cornejo Bravo, A. Serrano Medina, G.L. Pérez González, L.J. Villarreal Gómez, A summary of electrospun nanofibers as drug delivery system: drugs loaded and biopolymers used as matrices, Curr. Drug Deliv. 15 (10) (2018) 1360–1374, https://doi.org/10.2174/1567201815666180723114326 From NLM.

[21] J.-W. Yoo, D. Irvine, S. Mitragotri, Bio-inspired, bioengineered and biomimetic drug delivery carriers, Nat. Rev. Drug Discov. 10 (2011) 521–535, https://doi.org/10.1038/nrd3499.

[22] Y. Lu, J. Huang, G. Yu, R. Cardenas, S. Wei, E.K. Wujcik, Z. Guo, Coaxial electrospun fibers: applications in drug delivery and tissue engineering, WIREs Nanomed. Nanobiotechnol. 8 (5) (2016) 654–677, https://doi.org/10.1002/wnan.1391 (acccessed 2025/02/04).

[23] A. Luraghi, F. Peri, L. Moroni, Electrospinning for drug delivery applications: A review, J. Control. Release 334 (2021) 463–484, https://doi.org/10.1016/j.jconrel.2021.03.033.

[24] M. Souibgui, Z. Morávková, O.P. Georgievski, J. Hodan, M.A. Thottappali, V. Cimrová, J. Dvořáková, V. Proks, H. Studenovska, Ultrathin electrospun nanofibrous membranes based on poly(γ-benzyl-L-glutamate), J. Chem. Phys. 161 (23) (2024), https://doi.org/10.1063/5.0238633. From NLM.

[25] T. Ma, C. Tsai, S. Luo, W. Chen, Y. Huang, W. Su, Chemical structures and compositions of peptide copolymer films affect their functional properties for cell adhesion and cell viability, React. Funct. Polym. 175 (2022) 105265, https://doi.org/10.1016/j.reactfunctpolym.2022.105265.

[26] T. Ma, S. Yang, S. Luo, W. Chen, S. Liao, W. Su, Dual-function fibrous co-polypeptide scaffolds for neural tissue engineering, Macromol. Biosci. 23 (2) (2023) 2200286, https://doi.org/10.1002/mabi.202200286 (acccessed 2025/02/04).

[27] A.-J.A. Su, N. Jiang, S.-C. Luo, K.M. Washington, M.-C. Wu, Y.-C. Huang, W.-F. Su, Fibrous polypeptide based bioscaffold delivery of minocycline hydrochloride for nerve regeneration, Mater. Chem. Phys. 305 (2023) 127974, https://doi.org/10.1016/j.matchemphys.2023.127974.

[28] J. Wu, Z. Zhang, J. Gu, W. Zhou, X. Liang, G. Zhou, C.C. Han, S. Xu, Y. Liu, Mechanism of a long-term controlled drug release system based on simple blended electrospun fibers, J. Control. Release 320 (2020) 337–346, https://doi.org/10.1016/j.jconrel.2020.01.020 From NLM.

[29] G. Piccirillo, D.A. Carvajal Berrio, A. Laurita, A. Pepe, B. Bochicchio, K. Schenke-Layland, S. Hinderer, Controlled and tuneable drug release from electrospun fibers and a non-invasive approach for cytotoxicity testing, Sci. Rep. 9 (1) (2019) 3446, https://doi.org/10.1038/s41598-019-40079-7.

[30] A. Orlowska, P.T. Perera, M. Al Kobaisi, A. Dias, H.K.D. Nguyen, S. Ghanaati, V. Baulin, R.J. Crawford, E.P. Ivanova, The effect of coatings and nerve growth factor on attachment and differentiation of pheochromocytoma cells, Materials (Basel) 11 (1) (2017), https://doi.org/10.3390/ma11010060. From NLM.

[31] H. Zhu, R. Liu, Y. Shang, L. Sun, Polylysine complexes and their biomedical applications, Engineered Regeneration 4 (1) (2023) 20–27, https://doi.org/10.1016/j.engreg.2022.11.001.

[32] X. Ren, Y. Feng, J. Guo, H. Wang, Q. Li, J. Yang, H. Xuefang, J. Lv, N. Ma, W. Li, Correction: surface modification and endothelialization of biomaterials as potential scaffolds for vascular tissue engineering applications, Chem. Soc. Rev. 44 (2015), https://doi.org/10.1039/C4CS00483C.

[33] S. Purandare, R. Li, C. Xiang, G. Song, Development of innovative composite nanofiber: enhancing Polyamide-6 with ε-Poly-L-Lysine for medical and protective textiles, Polymers (Basel) 16 (14) (2024), https://doi.org/10.3390/polym16142046. From NLM.